Approximate description of the two-dimensional director field in a liquid crystal display

G. Panasyuk,[a] D. W. Allender, and J. Kelly
Liquid Crystal Institute and Department of Physics, Kent State University, Kent, Ohio 44242

(Received 19 October 2000; accepted for publication 2 February 2001)

A model for describing properties of a liquid crystal display which combines the concepts of in-plane switching and vertical alignment is proposed. There is good agreement between the results of this model and direct computer calculation of the director and the light transmittance. The usefulness of the model lies in the faster speed of calculations compared to direct computer solution of the Euler–Lagrange equations. © *2001 American Institute of Physics.*
[DOI: 10.1063/1.1359423]

I. INTRODUCTION

Recently several new types of liquid crystal displays (LCDs) with wide viewing angles, good color characteristics, and fast response times were proposed. Among them are a device associated with a homeotropic to multidomainlike (HMD) transition,[1,2] a liquid crystal (LC) π cell with patterned electrodes,[3] and an LCD cell which combines the concept of in-plane switching (IPS) with vertical alignment (VA).[4] In each of these examples there is a multidimensional director distribution, because the director depends on two or three space coordinates unlike the case of the usual twisted nematic displays. In our previous work[2] an approximate analytical approach for describing the HMD cell at high voltages was found. The purpose of this work is to develop an appropriate analytical model to describe the director configuration for an LCD which combines the concepts of IPS with VA for voltage differences, u, high enough that light transmittance is observable. The advantage of the model we have developed is that its calculational time is much faster than for direct computer solution. In addition, it can be generalized to describe other multidimensional LCDs such as the three-dimensional HMD cell, where a direct computer solution has not been carried out. It can be used, for example, for fast estimation of the optimal conditions for operation of these types of LCDs.

II. GENERAL IDEAS OF THE DESCRIPTION

In the cell studied in Ref. 4 vectors of the director **n** and electric field **E** always lie in a fixed plane (xz plane). The schematic diagram of this two-dimensional cell is shown in Fig. 1, where l is half the distance between adjacent electrode fingers and L equals $2l$ plus the width of an electrode finger. The thickness of the cell is d. The system possesses the following symmetries: (1) $2L$ periodicity along the x coordinate, (2) mirror symmetry with respect to the vertical yz planes at $x=\pm L/2$, $\pm 3L/2$,..., and (3) the electric potential $\Phi(x,z)$ is an odd function of x. Due to these symmetries it is sufficient to find the director only inside the region $0 \leqslant z \leqslant d$ and $0 \leqslant x \leqslant L/2$. The system possesses a series of wall defects. The central plane of one of these walls is the yz plane at $x=0$. Along this plane the electric field **E** is perpendicular to the initial (homeotropic) alignment, the torque due to the electric field is zero and the director stays homeotropic along the $x=0$ line even in the presence of **E**, as is illustrated in Fig. 1. Taking into account these symmetries, the free energy of the system per unit length in the y direction can be written as

$$F=\int_0^{L/2} dx\left[\int_0^d dz(F_d+F_f)-\frac{\epsilon_g}{8\pi}\left(\int_{-\infty}^0+\int_d^{\infty}\right)dzE^2\right], \quad (1)$$

where

$$F_d=\tfrac{1}{2}K_1(\partial_x\theta\cos\theta+\partial_z\theta\sin\theta)^2 + \tfrac{1}{2}K_3(\partial_z\theta\cos\theta-\partial_x\theta\sin\theta)^2 \quad (2)$$

and

$$F_f=-\frac{1}{8\pi}[\epsilon_a(\mathbf{n}\cdot\mathbf{E})^2+\epsilon_\perp E^2], \quad \epsilon_a=\epsilon_\parallel-\epsilon_\perp . \quad (3)$$

In these formulas $\theta(x,z)$ is the angle between the director **n** and $\hat{z}$ (we represent the director in the region $0\leqslant x\leqslant L/2$ and $0\leqslant z\leqslant d$ as $\mathbf{n}=\hat{x}\sin\theta-\hat{z}\cos\theta$). The dielectric constant for glass substrates is ϵ_g, K_1 and K_3 are the splay and bend elastic constants of the nematic, $\epsilon_\parallel$ and $\epsilon_\perp$ are values of the dielectric tensor parallel and perpendicular to the director, and the dielectric anisotropy is positive ($\epsilon_a>0$).

The main idea of the proposed model is to numerically solve the dynamic equation[5]

$$\gamma_1\partial_t\theta=-\delta F/\delta\theta \quad (4)$$

using the exact expression for the free energy (1) but an approximate expression for the electric field, which is found in this work. Here γ_1 is the rotational viscosity and flow is neglected. In contrast, previously used methods of direct computer calculation (e.g., the relaxation method[3,6,7]) do not use an approximate form for the electric field but instead solve $\nabla\cdot\mathbf{D}=0$ to get the electric field after each director update, based on Eq. (4).

[a]Electronic mail: georgy@columbo.kent.edu

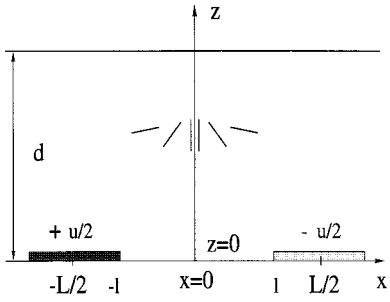

FIG. 1. Schematic diagram of the 2D cell.

It can be assumed that in most of the slab (except near the electrodes and wall defect layers of thicknesses of order of the correlation length ξ) the scale of spatial variations of $\mathbf{n}(\mathbf{r})$ is the same as for the electric potential. In this case, as can be seen from Eqs. (2) and (3), the characteristic value of the ratio F_d/F_f is determined by the parameter

$$\delta=\frac{4\pi K_m}{\epsilon_a(u)^2}, \tag{5}$$

where K_m is the maximum value of the elastic constants (K_3 in this case). To obtain an estimate of δ, we use the experimental value[4] of 5.2 for ϵ_a at 20 °C and 1 kHz and a typical value of 1.8×10^{-6} dyne for K_m. Thus if $u>1/30$ esu (10 V in *Système International*), $\delta<0.005$. Taking into account the condition $\mathbf{n}^2=1$ and neglecting the elastic energy completely, the Euler–Lagrange equations in the bulk in a zero order approximation can be written in the simple form:

$$-\frac{\epsilon_a}{4\pi}(\mathbf{n}\cdot\mathbf{E})\mathbf{E}=\lambda\mathbf{n}, \tag{6}$$

$$\nabla\cdot[\epsilon_\perp\mathbf{E}+\epsilon_a(\mathbf{n}\cdot\mathbf{E})\mathbf{n}]=0. \tag{7}$$

Equation (6) can be solved to obtain the following relationship between $\mathbf{n}$ and $\mathbf{E}$:

$$\mathbf{n}=\frac{\mathbf{E}}{E},\quad E=|\mathbf{E}|,\quad \lambda=-\frac{\epsilon_a E^2}{4\pi}, \tag{8}$$

which means that the director is parallel to $\mathbf{E}$. Substituting Eq. (8) into Eq. (7) we can write the equation for the electric potential:

$$\nabla\cdot(\epsilon_\parallel\mathbf{E})=0,\quad \text{or}\quad \nabla^2\Phi=0\quad \text{with}\quad \mathbf{E}=-\nabla\Phi, \tag{9}$$

assuming that $\epsilon_\parallel$, $\epsilon_\perp$ do not depend on $\mathbf{r}$.

Thus neglecting completely all the corrections produced by the presence of the layers near the substrate and the wall defect to the electric field (which are proportional to $\delta^{1/2}$ as was shown in Ref. 2 for the similar situation in the HMD cell), the electric potential for the zero order approximation Φ_0 can be found by solving the Laplace equation

$$\nabla^2\Phi_0=0 \tag{10}$$

with the following conditions on the electric field:

$$\Phi_0(\mathbf{r})=\pm\frac{u}{2}\ \text{ on the electrodes,}$$

and (11)

$$E_0(\mathbf{r})\to0\quad \text{when}\ \ |z|\to\infty,$$

where $\mathbf{E}_0=-\nabla\Phi_0$.

On the other hand, $\mathbf{n}(\mathbf{r})$ changes rapidly with characteristic scale determined by the electric correlation length $\xi(E_x)=(4\pi K_3/\epsilon_a)^{1/2}/E_x$ near the substrates and the $x=0$ plane to fit the homeotropic conditions there. Thus in a more realistic case when $\delta^{1/2}$ is small but not negligible, we have to take into account, in the general case, this small scale variation in the director and its influence on the electric field.

In Sec. II A we solve the boundary problem (10) and (11) to find the electric field in the zero order approximation, and in Sec. II B this solution will be modified to take into account changes of the director inside the substrate and wall defect layers.

A. Solution of the boundary problem

The general form of the solution of the Laplace equation is

$$\Phi_{\mathrm{LC}}=\sum_{p=0}^{\infty}[\alpha_p\exp(-s_{op}z)+\beta_p\exp(s_{op}z)]\sin s_p x$$

$$\text{where}\ \ s_{op}=s_p=(2p+1)\pi/L \tag{12}$$

inside the LC slab, and

$$\Phi_{g1}(\mathbf{r})=\sum_{p=0}^{\infty}\alpha_{1p}\exp(-s_pz)\sin s_px$$

and (13)

$$\Phi_{g2}(\mathbf{r})=\sum_{p=0}^{\infty}\alpha_{2p}\exp(s_pz)\sin s_px$$

in the glass for $z>d$ and $z<0$, respectively. Using the continuity of $\Phi(\mathbf{r})$ and of the normal component of the electric displacement vector $D_n(\mathbf{r})$ at the LC–glass interface at $z=d$ and continuity of $\Phi(\mathbf{r})$ at the $z=0$ glass–LC interface, one can express the β_p, α_{1p}, and α_{2p} coefficients in terms of α_p:

$$\alpha_{1p}=\frac{2\hat{\epsilon}\alpha_p}{(\hat{\epsilon}+1)},\quad \beta_p=e_p\alpha_p,\quad \alpha_{2p}=\alpha_p(1+e_p),$$

$$e_p=\frac{(\hat{\epsilon}-1)}{(\hat{\epsilon}+1)}\exp(-2s_{op}d), \tag{14}$$

where $\hat{\epsilon}=\epsilon_\parallel/\epsilon_g$. To determine all the coefficients α_p, β_p, α_{1p}, and α_{2p} completely, we introduce the electrode plane potential $V(x)$ which is continuous and a $2L$ periodic function of x has the values $\pm u/2$ on the electrodes, satisfies the symmetry relation $V(x)=V(L-x)$, and is an odd function: $V(x)=-V(-x)$. Using these conditions, $V(x)$ on the interval $-l\leqslant x\leqslant l$ may be written as

$$V(x)=-\frac{x}{2l}+\sum_{m=1}^{\infty}f_m\sin(\pi mx/l). \tag{15}$$

The number of f coefficients in the complete solution is of course infinite but an approximate solution may be found by truncating the series by some number $m_{\max} \equiv N$. Using the properties of $V(x)$, one can rearrange $V(x)$ in terms of $\sin s_p x$ and express all the coefficients (14) through $\{f_m\}$. To obtain the latter coefficients, the variational principle may be used to minimize the electric free energy F_f. Because Φ_{LC} and Φ_{vac} satisfy the Laplace equation and Φ_0 and D_n are chosen to be continuous at the upper interface at $z=d$, it is possible to rewrite F_f as the electrode plane functional:

$$F_f = \frac{1}{8\pi}\int_0^{L/2} dx(\epsilon_{\|}\Phi_{\mathrm{LC}}\partial_z\Phi_{\mathrm{LC}} - \Phi_{g2}\partial_z\Phi_{g2}) \quad \text{at } z=0. \tag{16}$$

Substituting here Eqs. (12) and (13) and integrating the resulting expression explicitly, we represent F_f as a quadratic form with respect to the arbitrary coefficients f_m. After that, differentiating F_f with respect to these coefficients and equating the results to zero, we will get the following system of linear inhomogeneous algebraic equations with respect to f_m:

$$\sum_{n=1}^{N} y_{mn} f_n = r_m, \quad m = 1,2,\ldots,N. \tag{17}$$

In this system

$$y_{mn} = \sum_{p=0}^{\infty} b_{mp} b_{np} B_p, \quad r_m = -\sum_{p=0}^{\infty} A_p b_{mp} B_p, \tag{18}$$

where

$$\begin{aligned} B_p &= s_{op} d\left[\hat{\epsilon}\frac{(1-e_p)}{(1+e_p)} + 1\right], \\ A_p &= -\frac{2\sin[(2p+1)\pi\bar{l}]}{\bar{l}\pi^2(2p+1)^2}, \quad \bar{l} = \frac{l}{L}, \end{aligned} \tag{19}$$

and

$$\begin{aligned} b_{np} = \{1/[(2p+1)\bar{l} - n] - 1/[(2p+1)\bar{l} + n]\}\frac{2\bar{l}}{\pi} \\ \times \sin[(2p+1)\pi\bar{l}], \end{aligned} \tag{20}$$

where A_p and b_{np} are the Fourier coefficients which arise after rearrangement of $V(x)$ in terms of $\sin s_p x$. One important observation must be made about the system (17). It becomes inconvenient to solve Eq. (17) exactly for large N. On the other hand, because of nonanalyticity of the electric potential near the sharp edges of the electrodes, an accurate description of the electric field requires $N \geqslant 50$. Fortunately, the matrix $\hat{Y} = \{y_{mn}\}$ in Eq. (17) can be represented as $\hat{Y}_0 + \Delta\hat{Y}$, where $\hat{Y}_0$ is diagonal and $\Delta\hat{Y}$ is small with respect to $\hat{Y}_0$. Thus we can solve Eq. (17) by means of an iterative procedure

$$\mathbf{f}_N^{(n)} = \hat{Y}_0^{-1}(\mathbf{R} - \Delta\hat{Y}\mathbf{f}_N^{(n-1)}) \tag{21}$$

for $n \geqslant 1$, which has rapid convergence for any reasonable N. In Eq. (21) $\mathbf{f}_N$ and $\mathbf{R}$ designate two sets $\{f_m\}$ and $\{r_m\}$ of N elements each.

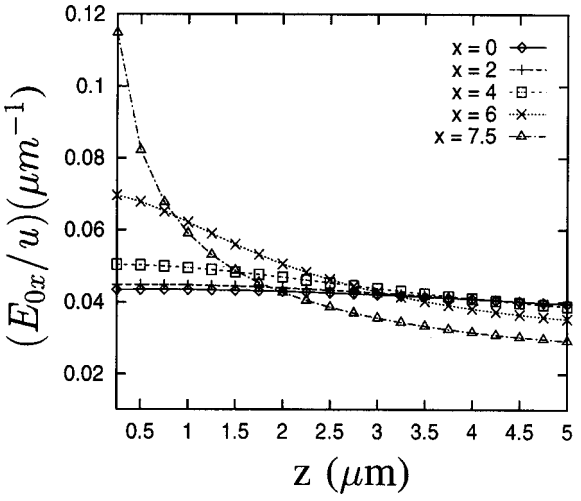

FIG. 2. Graph showing the z dependence of E_{0x} at different values of the x coordinate.

B. Modifications of the electric field caused by variation of the director on short length scales

In this section we are going to estimate the influence of the near-substrate and wall defect layers on the zero order solution $\mathbf{E}_0$. In all the displays mentioned in the Introduction, d is much less than L (usually $d/L \leqslant 0.2$). Thus if wall defect layers were not present, all terms with x derivatives in the Euler–Lagrange equations for the director and electric field could be neglected. This gives us

$$\begin{aligned} K_b(\theta)\partial_{zz}^2\theta - \tfrac{1}{2}\Delta K \sin(2\theta)(\partial_z\theta)^2 \\ + \frac{\epsilon_a}{4\pi}\left[\frac{1}{2}(E_x^2 - E_z^2)\sin 2\theta - E_x E_z \cos 2\theta\right] \approx 0, \end{aligned} \tag{22}$$

$$\partial_z[\epsilon_\perp E_z - \epsilon_a(\mathbf{n}\cdot\mathbf{E})\cos\theta] \approx 0, \tag{23}$$

where $K_b(\theta) = K_1 \sin^2\theta + K_3\cos^2\theta$ and $\Delta K = K_3 - K_1$. Neglecting x derivatives in the Maxwell equation $\nabla\times\mathbf{E} = 0$ shows that one can also neglect the $\mathbf{z}$ derivative of E_x in Eq. (23). It means that small length scale changes in the director field near a substrate having homeotropic boundary conditions do not produce the same significant changes in E_x. In such a situation E_x is close to its zero order approximation: $E_x \approx E_{0x}$. Figure 2 shows the z dependences of E_{0x} for different values of x throughout the most important region between (nontransparent) electrodes, $x < l$. As illustrated in Fig. 2, z dependences are really weak everywhere except in the vicinity of the electrode edge at $x = l$. In the small region $x \approx l$, however, the electric field is very strong, the correlation length is small, and the director is approximately parallel to the electric field as described by Eq. (8). Thus $\mathbf{E} \approx \mathbf{E}_0$ near $x = l$. Taking the constant of integration in Eq. (23) as the value of the expression in square brackets at a particular point $z = z_m$ $(0 < z_m < d)$ and using the approximation $E_x \approx E_{0x}$, one can rewrite Eq. (23) after integration in the following form:

$$E_z \approx \frac{2(\epsilon_\perp + \epsilon_a\cos^2\theta_m)E_{zm} + \epsilon_a(\sin 2\theta E_{0x} - \sin 2\theta_m E_{0xm})}{2(\epsilon_\perp + \epsilon_a\cos^2\theta)}, \tag{24}$$

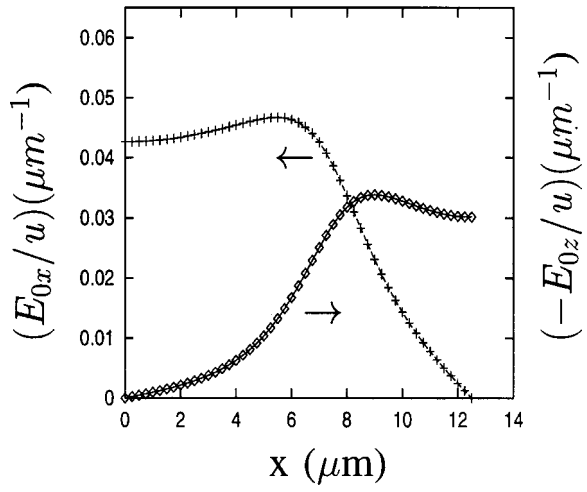

FIG. 3. Electric field components $-E_{0z}(x,z=d/2)$ and $E_{0x}(x,z=d/2)$. Equation (26) indicates E_z is significantly different from E_{0z}, but the comparison $|E_z| \ll E_{0x}$ for small x is still correct.

where $E_{zm}=E_z(x,z_m)$, $E_{0xm}=E_{0x}(x,z_m)$, and $\theta_m=\theta(x,z_m)$, and z_m can be chosen from the following considerations. As was shown before,[2] for relatively large voltages (more than $u_0 \approx 10\,\mathrm{V}$ for the experimental set of cell parameters[4] which is pointed out in Sec. III) it is possible to provide a reasonable description of the slab by dividing it into two near-substrate layers with thicknesses $\Delta_1 \approx \Delta_2 \approx 2\xi$ and a bulk region between them where $\mathbf{E}$ is close to $\mathbf{E}_0$. It means that one can choose $E_{zm} \approx E_{0zm}=E_{0z}(x,z_m)$ in Eq. (24) with z_m close to $d/2$. Indeed, our calculations show that the director distribution for $u>10\,\mathrm{V}$ does not depend significantly on z_m if it is taken from the interval $0.35d \leqslant z_m \leqslant 0.6d$. However, as u is lowered, the bulk region shrinks and finally disappears when $u<u_0$, where u_0 can be estimated from the relation $4\xi=d$ with $\xi \approx \xi(E_{0x})$. The most important consequence of this is that E_z deviates significantly from E_{0z} for these voltages even in the central part of the slab for $x<l/2$, and there is no value of z_m for which $E_{zm} \approx E_{0zm}$ with a good accuracy in Eq. (24). It means that formula (24) fails to describe E_z properly for $u<u_0$ for the important region of small x. At first sight it is not important to know E_z accurately for the director calculations because $|E_z| \ll E_x \approx E_{0x}$, which is illustrated in Fig. 3. But this is a wrong impression. The problem is that for small x, when $\cos 2\theta \approx 1$ and $\sin 2\theta \approx 2\theta$, $|E_z|E_{0x}$ is comparable to $0.5(E_{0x}^2 - E_z^2)\sin 2\theta \approx E_{0x}^2\theta$ in the electric field contribution to the Euler–Lagrange equation for θ [see the last term in Eq. (22)].

To estimate E_z properly, let us consider again a solution of Eq. (23) (without assuming any particular value for E_{zm}) for small $x<x_1$, where x_1 is the largest value of the x coordinate for which the following approximate relations $\epsilon_\perp + \epsilon_a \cos^2\theta \approx \epsilon_\parallel$ and $\sin 2\theta \approx 2\theta$ are still satisfied within about 10% accuracy, which means that θ is less than about $\theta_1 \approx 0.4$ for all realistic values of $\epsilon_\parallel$ and $\epsilon_\perp$ [x_1 is a function of u and the other cell parameters and is found from the condition $\theta(x_1,d/2)=\theta_1$ in the course of solving Eq. (4)]. Using these approximate relations, one can rewrite Eq. (23) as

$$\partial(\epsilon_\parallel E_z - \epsilon_a \theta E_{0x}) \approx 0, \tag{25}$$

which allows us to assume the following form for $E_z(x,z)$ in the region $x<x_1$:

$$E_z(x,z)=\frac{\epsilon_a}{\epsilon_\parallel}\theta(x,z)E_{0x}(x,z)+e, \tag{26}$$

where e does not depend on z or its z dependence is much weaker than in the first term in Eq. (26). Because $\theta \propto x$ due to the presence of the wall defect and $E_z \propto x$ due to the symmetry of the problem when $x \to 0$, e must behave also like αx at small x. To determine e, let us notice, that for $u \to 0$, the amplitude θ_a of the θ distribution also goes to zero ($\theta_a \propto u^2$ when $u \to 0$, as follows from the Euler–Lagrange equation for θ). Thus one can assume that $e=E_{0z}^l$, where $\mathbf{E}_0^l \equiv (E_{0x}^l, E_{0z}^l)$ is the low voltage asymptotic value of the electric field, which can be found as a solution of the boundary problem for the corresponding low voltage potential $\Phi_0^l(\mathbf{r})$:

$$\epsilon_\perp \partial_x^2 \Phi_0^l + \epsilon_\parallel \partial_z^2 \Phi_0^l = 0 \tag{27}$$

with the same conditions (11) on the electric field:

$$\Phi_0^l(\mathbf{r}) = \pm\frac{u}{2} \quad \text{on the electrodes,}$$

and (28)

$$E_0^l(\mathbf{r}) \to 0 \quad \text{when} \quad |z| \to \infty,$$

where $\mathbf{E}_0^l = -\nabla\Phi_0^l$. Equation (27) is the Maxwell equation $\nabla\cdot\mathbf{D}=0$ with $\theta \equiv 0$ everywhere inside the cell. The solution of this boundary problem (27) and (28) can be described in the same way as was done in Sec. II A with the same value of s_p and the following substitutions: $\Phi_{\mathrm{LC}} \to \Phi_{\mathrm{LC}}^l$, $\Phi_{g1} \to \Phi_{g1}^l$, $\Phi_{g2} \to \Phi_{g2}^l$, $\hat{\epsilon} \to \hat{\epsilon}_1 = \hat{\epsilon}(\epsilon_\perp/\epsilon_\parallel)^{1/2}$, and $s_{0p} = s_p(\epsilon_\perp/\epsilon_\parallel)^{1/2}$.

Thus one can approximate E_z in the interval $0 \leqslant x \leqslant x_1$ by Eq. (26), where

$$e = E_{0z}^l. \tag{29}$$

Indeed, our calculations show that the z dependence in E_{0z}^l is weaker than in $\theta(x,z)$; besides, for all voltages important for light transmittance a contribution of the first term in Eq. (26) for $z \approx d/2$ is more than an order of magnitude larger than E_{0z}^l. This notice justifies the form of E_z given in Eq. (26).

For $x_1<x<x_l \approx 0.8l$, $\sin 2\theta$ is comparable to (or even larger than) $|\cos 2\theta|$, and, because $|E_z| \ll E_x$, accurate values for E_z are not important for this region. For x close to l, the electric field is strong even for the lowest voltages of interest, and $\mathbf{E} \approx \mathbf{E}_0$, as was already mentioned. For $l<x \leqslant L/2$, E_z is the largest component of $\mathbf{E}$, θ is small, and one can also assume that $E_z \approx E_{0z}$ in that region. Comparison with the results of direct computer calculation for $\mathbf{E}$ shows that $E_x \approx E_{0x}$ throughout the cell with an accuracy about 10%, and $E_z \approx E_{0z}$ for $x>0.8l$ with the same accuracy. These considerations allow us to use formula (24) for E_z with $z_m \approx d/2$ for $x_1<x \leqslant L/2$. Thus for the case of relatively low voltage ($u<u_0 \approx 10\,\mathrm{V}$ for the experimental cell), x_1 is relatively large ($x_1 \propto l/2$), and using E_z from Eqs. (26) and (29) on the interval $0 \leqslant x \leqslant x_1$ instead of Eq. (24) is very important. Figure 4 shows a result of calculation of x dependence of E_z for

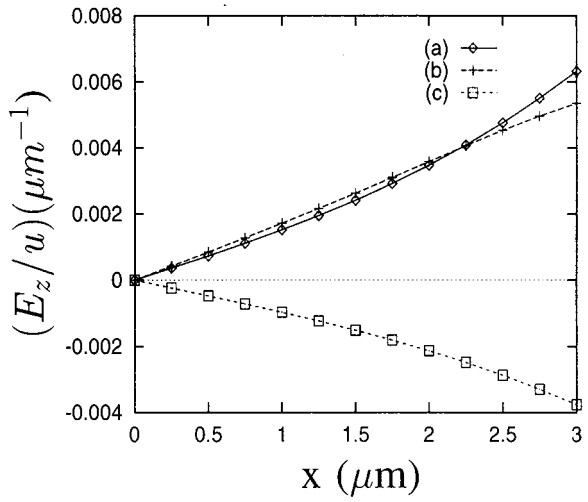

FIG. 4. Electric field component $E_z(x,z=d/2)$ at $u=9$ V obtained from (a) Eqs. (26) and (29), (b) direct computer calculation, and (c) Eq. (24) with $z_m=d/2$.

some $u<u_0$ for $x<x_1$ in accordance with Eqs. (26) and (29) [curve (a)]. This result is in reasonable agreement with the corresponding results of direct computer calculation, but deviates significantly (even has a different sign) from a result produced by the application of Eq. (24) with $z_m=d/2$ [curve (c)]. As one finds from Fig. 4, E_z is positive in the central region of the cell, whereas both E_{0z} and E_{0z}^l are negative. As indicated by Eq. (26), this interesting effect is due to the anisotropy of LCs and disappears when $\epsilon_a \to 0$. When u increases, x_1 decreases quickly, and formula (24) is applicable for nearly all x. On the other hand, when voltage increases, E_z approaches E_{0z} and $E_z \approx E_{0z}$ even for small x.

To understand the influence of the wall defect layer on E_x, let us consider the following ideas. Because $|E_z|$ is relatively small for $x \leqslant 2\xi \equiv \Delta_w$, it is reasonable to use $E_z=0$ there when determining the influence of the wall defect on E_x. Again, the equation $\nabla \times \mathbf{E}=0$ implies that we can neglect the z dependence of E_x for the small x region. Thus one can rewrite the equation $\nabla \cdot \mathbf{D}=0$ as

$$\partial_x[E_x(\epsilon_\perp+\epsilon_a \sin^2\theta)]-\epsilon_a E_x \partial_z(\sin\theta\cos\theta)\approx 0. \tag{30}$$

Considering Eq. (30) as an ordinary differential equation with respect to $E_x=E_x(x)$, one can solve it along the line $z=d/2$, where the last term in Eq. (30) can be neglected (because $\partial_z\theta \approx 0$ along the line $z=d/2$, see the Appendix). Representing the integration constant of the resulting equation as a value of the expression in square brackets in Eq. (30) at the point $x=\Delta_w$, one can write the solution for E_x as

$$E_x = g(x)E_x', \quad g(x)=\frac{\epsilon_\perp+\epsilon_a \sin^2\theta_0}{\epsilon_\perp+\epsilon_a \sin^2\theta}, \tag{31}$$

where $\theta_0=\theta(\Delta_w,d/2)$ and $E_x'=E_x(\Delta_w,d/2)$. On the other hand, when x increases, the role of x-derivatives decreases, and the director distributions can be found from Eq. (22) where, however, a bulk electric field distribution (electric field far from the plane $x=0$, which is close to $\mathbf{E}_0$) must be modified by the presence of the wall defect layer. In particular, one has to replace $\mathbf{E}_0$ for the part of the cell outside the wall defect layer by a modified field $\mathbf{E}_0' \equiv (E_{0x}', E_{0z}')$, which means that E_x' in Eq. (31) can be approximated by $E_{0x}'(\Delta_w, d/2)$. Note that for typical values of $\epsilon_\perp$ and ϵ_a (see, for example, their experimental values in Sec. III) and $60° < \theta_0 < 90°$ (for $u>12$ V) E_x at $x=0$ can be about twice E_x' $\approx E_{0x}'(\Delta_w, d/2)$.

To determine E_{0x}', let us consider a modified cell at the same voltage which reproduces the electric field $\mathbf{E}_0'$ at large x by means of the zero order method (as described in Sec. II A). As we know (see, for example, Fig. 2), the zero order field component E_{0x}' varies slowly at small x, which means that $E_{0x}'(0,z) \approx E_{0x}'(\Delta_w, z)$ for any z. If the cell was not modified, the modified field $\mathbf{E}_0'$ would describe the cell at a lower voltage, because $E_{0x}' < E_x$ for $x<\Delta_w$ [see Eq. (31)] and $\mathbf{E} \approx \mathbf{E}_0'$ for larger x. In order for the modified cell to have the same voltage drop, it must have extended dimensions $L'=L+2\,\delta x$ and $l'=l+\delta x$ (and the same d) with some $\delta x>0$. This cell can be produced from the region $0 \leqslant x \leqslant L/2$ and $0 \leqslant z \leqslant d$ of the cell under consideration by shifting the value of x where the potential $\Phi=0$ (see Fig. 1) to the left by δx and using the symmetry and periodicity properties to extend the solution to all $\mathbf{r}$. Calculating the corresponding integral $\Delta\Phi'$ for the defect layer using the expression (31) for E_x, one finds an equation for δx:

$$\Delta\Phi' = E_{0x}'(\Delta_w+\delta x). \tag{32}$$

Finally, δx, E_{0x}', and E_{0z}' can be determined self-consistently in the following way. Choosing some arbitrary δx (for example, $\delta x=0.1l$) and taking $L'=L+2\,\delta x$ and $l'=l+\delta x$, one calculates $\mathbf{E}_0'$, as described in Sec. II A. Then, using this $\mathbf{E}_0'$ and the expression (A9) for δx from the Appendix [which follows from Eq. (32)] one calculates a δx. In general the calculated δx will differ from the initial choice of δx, so the calculational procedure must be repeated several times until convergence is achieved. Details of the calculation are given in the Appendix.

Let us discuss some important results concerning the electric field $\mathbf{E}_0'$. Our calculations show that E_{0z}' always coincides with E_{0z} within 1% to 3% accuracy. Figure 5 illustrates characteristic results for the calculation of E_x using the model scheme described above [curve (a)], and also for comparison of the corresponding result determined by direct computer calculation [curve (b)]. As is shown in Fig. 5 [curve (a)], E_x increases significantly from E_{0x}' when x decreases toward zero, which is at least in qualitative agreement with the result of the direct computer calculation. As voltage u decreases, the peak in E_x centered at $x=0$ decreases and practically disappears when $u \leqslant u_0$ (for the experimental set of cell parameters, $u_0 \approx 10$ V). The latter result can be understood easily, using Eq. (31) and taking into account that θ_0 in Eq. (31) also becomes small, and $g(x)$ approaches 1 when u decreases. As follows from Eq. (A9) of the Appendix, when $u \to \infty$, δx decreases, because θ_0 cannot exceed $\pi/2$ and $E_{0x}' \propto u \to \infty$. Therefore l' and L' approach the cell values l and L, $\mathbf{E}_0'$ approaches $\mathbf{E}_0$, and the increase of E_x towards the point $x=0$ also goes to zero when $u \to \infty$.

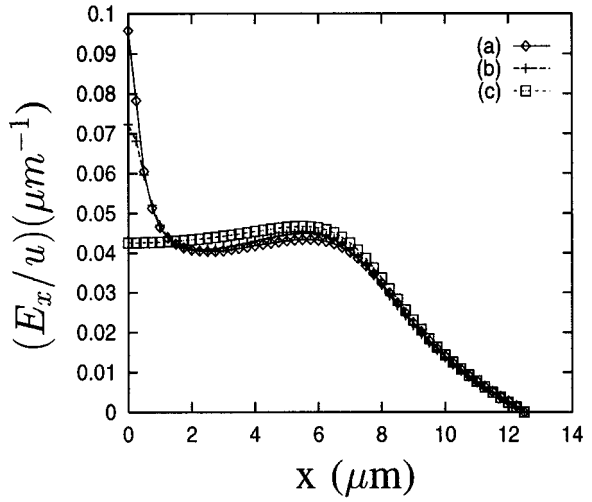

FIG. 5. Electric field component $E_x(x,z=d/2)$ at $u=16$ V obtained from (a) Eqs. (31) and (32), (b) direct computer calculation, and (c) zero order solution E_{0x}.

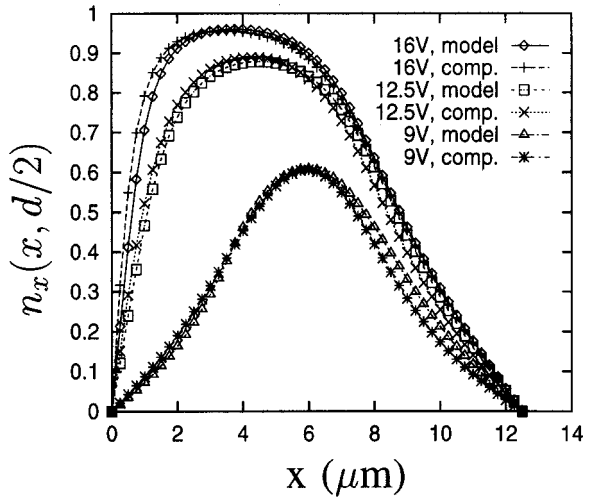

FIG. 6. Director component $n_x(x,z=d/2)$ at 9, 12.5, and 16 V as calculated by the model and by direct computer calculation.

As one finds from Fig. 5, the values of E_{0x} are significantly lower than the calculated E_x values for both the model and direct computer calculations when $0 \leqslant x < \Delta_w$, and slightly higher for the large x part of the cell. However, we find that this difference between E_{0x} and E_x usually produces only small changes in the corresponding director distributions. It means that the result of the director field calculation from the dynamic Eq. (4) is relatively stable with respect to small variations of the electric field, used in Eq. (4). The most important consequence of this statement is that one can simplify significantly the expression for the electric field, used in the director calculations. In particular, one can approximate $E_x \approx E_{0x}$ and use expressions (24), (26), and (29) for E_z. It is worth mentioning that the use of the approximate field expressions in the course of solving Eq. (4) speeds up the calculation by a factor of about 30 with respect to the direct computer solution for the two-dimensional problem being considered here.

III. RESULTS AND DISCUSSION

The results of the director calculation and the resulting optical properties are illustrated in Figs. 6–9. For each of these figures we used the following set of experimental cell parameters:[4] $K_1=13.2$ pN, $K_3=18.3$ pN, $\epsilon_\perp=3.1$, $\epsilon_\parallel=8.3$, $L=25\,\mu$m, $d=5\,\mu$m, and $l=7.5\,\mu$m. Figure 6 shows the x dependence of $n_x=\sin\theta(x,d/2)$ for several voltages as calculated in two different ways: (a) our model [based on Eqs. (4), (24), (26), (29), and the approximation $E_x \approx E_{0x}$] and (b) direct computer calculations (relaxation method[6,8]). In the latter case the Maxwell equation $\nabla\cdot\mathbf{D}=0$ together with Eq. (4) are solved numerically. After discretizing $\nabla\cdot\mathbf{D}=0$, an equation linear in the discretized values of the voltage can be solved to yield an update formula for the potential $\Phi(x_i,z_k)$ at the current grid point (x_i,z_k) after each iteration of Eq. (4) for the director. Because of the symmetries of the problem, namely mirror symmetry $\Phi(L/2-x,z)=\Phi(x,z)$ and the relation $\Phi(x=0,z)=0$, we solved the equation $\nabla\cdot\mathbf{D}=0$ only on the interval $0 \leqslant x \leqslant L/2+\Delta x$, where $\Delta x=\Delta z=0.25\,\mu$m was the mesh step in both x and z directions inside the LC slab, with the boundary condition $\Phi=-u/2$ on the electrode. To take into account the boundary conditions at $z=\pm\infty$, it is important to use the results of Sec. II A that the spatial scale for the decay rate of the electric field inside the glass substrates is of order L. In particular, the decay rate of the lowest harmonic is π/L. Therefore we use a uniform mesh inside both glass substrates with boundary conditions $\partial_z\Phi=0$ at $|z_b|=2L$ and mesh steps $\Delta x_g=\Delta x$ and $\Delta z_g=2\Delta x$ inside the glass layers. We also used a logarithmic mesh[9] inside the glass substrates for comparison and set $\Phi=0$ at $z=\pm 40L$. We found, however, that the relative difference in the results of the director calculations using these two meshes inside the glass layers is very small (less than 0.1%). On the other hand, if one takes a finer mesh with all mesh steps decreased by a factor of 2, namely, $\Delta x'=\Delta z'=0.125\,\mu$m in the LC cell and $\Delta z'_g=2\Delta z'$ and $\Delta x'_g=\Delta z'$ inside the glass substrates (in the case of a uniform mesh), there are somewhat larger changes in the director distribution. In particular, we found a difference of about 0.2% to

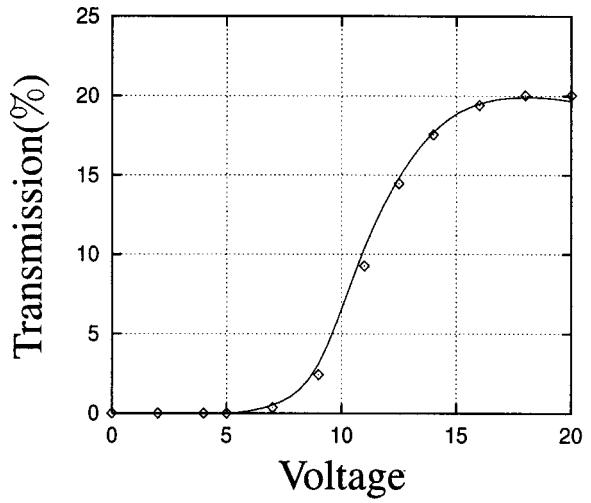

FIG. 7. Optical transmission vs voltage. The solid curve is calculated using the model and the dots are obtained from direct computer calculation.

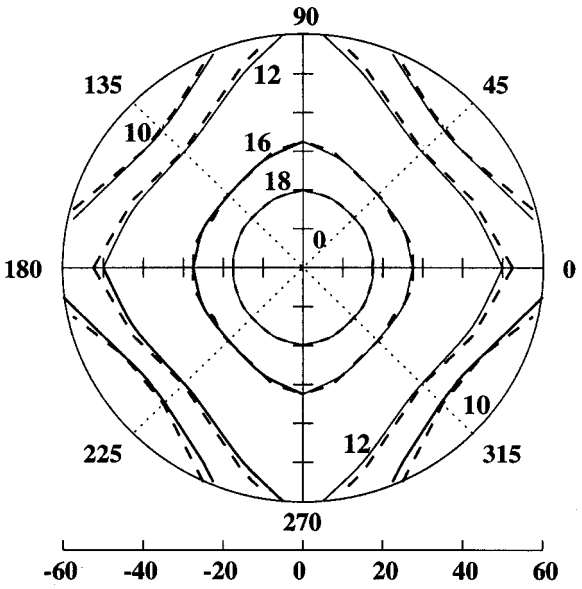

FIG. 8. Isocontrast contour plots. The solid lines correspond to the direct computer calculation and the dashed lines to the model.

0.5% in the amplitude values θ_a for the director angle for all voltages considered here, and about 2% to 3% for values of θ inside the wall defect and substrate layers where θ rises steeply from its zero value at the substrates and the $x=0$ plane for the case of large voltages. This is our estimate for the error of the direct computer calculations for the 0.25 μm mesh, used here in all figures for comparison with the model.

The program for the direct computer calculation was checked carefully by comparing with some special cases, where the results are known. One of them is the case of interdigitated electrode fingers surrounded by a uniform dielectric. The electric field for this case can be produced with very good accuracy (with an error of less than 0.1%) in a way described in Sec. II A with the substitution $\epsilon_{\parallel}=\epsilon_{\perp}=\epsilon_g$. The result of the direct computer solution corresponds to this analytical solution. Another case is the low voltage

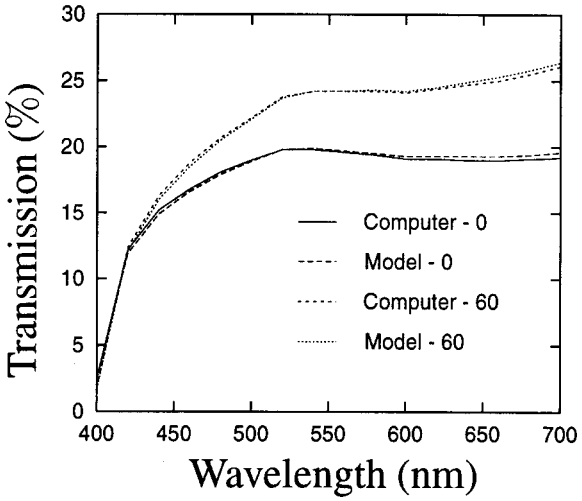

FIG. 9. Optical transmission vs wavelength. The curves are for two angles of incidence (0° and 60°) and are obtained by two different calculational methods.

asymptote for the electric field $\mathbf{E}_0^l=-\nabla\Phi_0^l$, which is found analytically in Sec II B. This asymptote is valid when u is so small that $E_x\sin\theta\approx E_{0x}^l\theta\ll E_z\approx E_{0z}^l$ for all space coordinates inside the cell. Our calculations show that $\theta E_{0x}^l/E_{0z}^l<0.01$ only if $u<0.7$ V (for the experimental set of cell parameters). We find that our direct computer calculation program produces the expected results $\mathbf{E}=\mathbf{E}_0^l$ for these low voltages. The final check of the program is a comparison of the calculated electric field and director with the electric field $\mathbf{E}_0$ and director solution $\mathbf{n}_0=\mathbf{E}_0/E_0$, found analytically in Sec. II and valid for high voltages. The basis for this comparison is that when $u\to\infty$, the near substrate layers and the wall defect layer shrink, the director becomes parallel to $\mathbf{E}$, and the electric field and director approach their zero order analytical solutions $\mathbf{E}_0$ and $\mathbf{n}_0$ at the central region of the LC cell (outside the layers). Our calculations show that the results of the direct computer solution program also agree with this limit.

The program for the direct computer solution also reproduces the director field, calculated by the model after substituting $\mathbf{E}_0^l$ into the dynamic equation (4) with an expected accuracy $O(\theta E_{0x}^l/E_{0z}^l)$ for low voltages, and the director, calculated after substituting $\mathbf{E}_0$ into Eq. (4) for the high voltage limit.

As is clear from Fig. 6 we have good agreement between the model and direct computer calculations for the LC display application voltage interval $7<u<20$ V, which the optical results of Figs. 7–9 show is the range of interest. Figures 7–9 illustrate results of calculations of the light transmittance based on the geometrical optics approach (GOA), using a director pattern as input. The application of GOA to one-dimensional modeling of inhomogeneous LCs was originally done by Ong and Meyer[10] and applied extensively by Ong.[11,12] A generalization of GOA to the multidimensional cells was described in Ref. 4. In particular, Fig. 7 shows the voltage-dependent optical transmittance for normal incidence using director patterns obtained by our model and by direct computer calculation. Figures 8 and 9 display the same comparison for an isoluminance contour plot and wavelength-dependent light transmittance at $u=16$ V. In Fig. 8 contours are labeled by percent transmission. The solid lines correspond to the direct computer calculation and the dashed lines to the model. Agreement between the two director profiles is good even for a polar angle higher than 40°. Figures 7 and 8 are plotted for normal incidence, and the light source is white light. Figure 9 displays the transmission versus wavelength curves for the direct computer and model calculations, and data are shown for two angles of incidence: 0° and 60°. The plane of incidence is the plane of the director.

An interesting question is connected with the wall defect structure. An alternative to the wall defect is two disclination lines with strengths $m=\pm 1/2$ at some distance $\Delta\propto\xi$ from the top and bottom substrates which lie in the $x=0$ plane and are parallel to the substrates.[2] The energy W_w of the wall defect and the energy W_l of the disclination lines (per unit length in the horizontal y direction) can be estimated[5,13,14] as

$$W_w\approx\frac{2Kd}{\xi} \tag{33}$$

and

$$W_l = 2\pi m^2 K\left(\log\frac{R}{r_c}+\alpha\right)+2\frac{2K\Delta}{\xi} \tag{34}$$

in a one elastic constant approximation[5] [here $K=(K_1+K_3)/2$]. In the last formula $\pi m^2 K \log(R/r_c)$ is the macroscopic energy of elastic deformation associated with one line. A characteristic size R of the deformation can be taken as $R\approx\xi$, and r_c is the radius of the defect core (r_c is of the order of a molecular size, 2 nm).[5] Further the core energy is $\pi m^2 K\alpha$, where α can vary between 0 and $\log R/r_c$.[13–15] The last term in Eq. (34) is the energy associated with two small wall defects which lie in the $x=0$ plane and connect the defect lines to the substrate planes. Because both of these two lengths Δ and ξ are inversely proportional to the electric field, this last term does not depend on voltage, and W_l increases with voltage very slowly (logarithmically). On the other hand W_w is proportional to u. This means that when u becomes larger than some critical voltage u_c, which can be found from the equation

$$W_w = W_l, \tag{35}$$

a first order phase transition to the alternative defect structure with two disclination lines occurs. From Eq. (35) u_c is estimated to be between 20 and 40 V depending on the particular value of α. On the other hand, only the wall defect structure has been observed in experiments[4] on this cell, at least for voltages below 60 V. Because the line defect structure has not been seen, no attempt was made to develop a fast calculation model for such a structure. The absence of the disclination lines in the experiment needs further consideration, but may be due to energy barriers encountered in transforming from a wall defect to disclination lines.

IV. CONCLUSIONS

A simplified model was constructed to describe the director configuration in a two-dimensional (2D) cell with interdigitated electrodes. The simplified model provides an alternative to the traditional method of direct computer solution of the Euler–Lagrange equations for the director and electric field in analyzing behavior of liquid crystal cells. Calculations show good agreement between results of this model and direct computer calculation of the director. Corresponding results for the light transmittance, based on the director patterns provided by the model and direct computer calculations, are in good agreement as well. The model also helps to understand some interesting features in the electric field distribution important for display applications, such as the behavior of the electric field component normal to the substrate in the region midway between the interdigitated electrodes for relatively low voltages. Another advantage of the model is that its calculational time is about 30 times faster than for the direct computer solution. A preliminary study indicates that it can be generalized to describe the three-dimensional (3D) HMD cell.[1,2] As follows from the geometry of the HMD cell,[2] the electric field component perpendicular to the wall defect layer is negligible (unlike the 2D case) and one can neglect the influence of the wall defect layer on the electric field. Using the particular symmetries of that cell[2] and this observation, one can construct a 3D variant of the model described in this work.

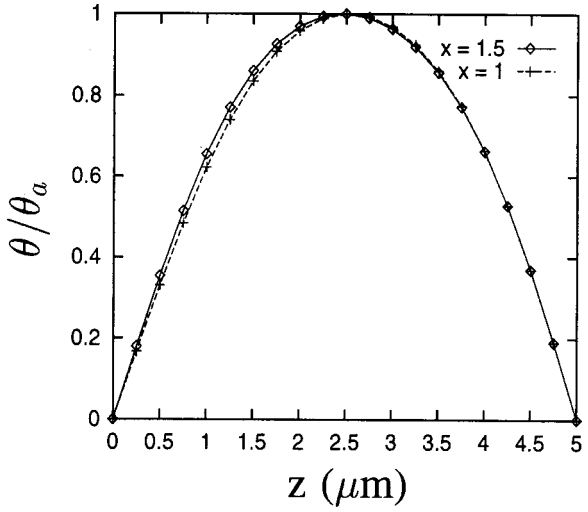

FIG. 10. Graph showing z profiles of θ for $x=1.5$ and 1 μm at $u=16$ V.

ACKNOWLEDGMENTS

This work was supported by the National Science Foundation under the Science and Technology Center ALCOM DMR89-20147. We would like also to acknowledge Dr. Leo Holmberg for his help in optimization of the programming tools important for the present research.

APPENDIX

Substituting the expression $E_x = g(x)E'_{0x}$ into Eq. (32) one can rewrite it as

$$(\Delta_w+\delta x)E'_{0x} = \int_0^{\Delta_w} dx\,\frac{(a-\cos 2\theta_0)}{(a-\cos 2\theta)}E'_{0x} \tag{A1}$$

with $a=2\epsilon_\perp/\epsilon_a+1$. Because E'_{0x} depends weakly on x at small x, this simplifies to

$$\delta x = \int_0^{\Delta_w} dx\,\frac{(\cos 2\theta-\cos 2\theta_0)}{(a-\cos 2\theta)}. \tag{A2}$$

To estimate this integral, let us consider the Euler–Lagrange equation $\delta F/\delta\theta=0$ along the line $z=d/2$ for $x\leqslant\Delta_w$. We assume that the function $\theta_a(x)\hat{\theta}(z/\Delta)$ gives an accurate representation for $\theta(x,z)$, the angle of deviation from the homeotropic state. Here $\hat{\theta}$ is called the z profile and it is normalized to have a value of one at $z=\Delta$, and $\theta_a(x)$ gives the maximum value of θ at a given x as z varies over the sample thickness. The validity of this assumption is illustrated in Fig. 10. Both the z profile and the parameter Δ are slow functions of x inside the wall defect region, and Δ is close to $d/2$ (which means, in particular, that $\partial_z\theta\approx 0$ along the line $z=d/2$ in the wall defect region). These curves were obtained by solving Eq. (4) using the approximate expression for **E** found in Sec. II [see, in particular, Eqs. (24), (26), (29), (31), and (32)]. Analogous direct computer calculations give very similar results. Neglecting all terms with a first z de-

rivative [such as $(\partial_z\theta)^2$, $\partial^2_{xz}\theta$, and $\partial_x\theta\partial_z\theta$] and neglecting E_z as was discussed preceding Eq. (30), one can rewrite the equation $\delta F/\delta\theta=0$ as

$$K_a(\theta)\partial^2_{xx}\theta+K_b(\theta)\partial^2_{zz}\theta+\tfrac{1}{2}\Delta K\sin 2\theta(\partial_x\theta)^2+\frac{\epsilon_a}{8\pi}E_x^2\sin 2\theta \approx 0, \tag{A3}$$

where $K_a(\theta)=K_3\sin^2\theta+K_1\cos^2\theta$, $K_b(\theta)=K_1\sin^2\theta+K_3\cos^2\theta$, and $\Delta K=K_3-K_1$. The term with $\partial^2_{zz}\theta$ in this equation can be determined by recalling that the z dependence of θ at small x is nearly the same as the z dependence for x close to Δ_w and therefore using the large x form of Eq. (A3), where one can neglect all x derivatives and put $E_x\approx E'_{0x}$:

$$K_b(\theta)\partial^2_{zz}\theta+\frac{\epsilon_a}{8\pi}E'^2_{0x}\sin 2\theta\approx 0. \tag{A4}$$

Equation (A4) is applicable in the region z near $d/2$ and x near Δ_w. Substituting $\partial^2_{zz}\theta$ from Eq. (A4) into Eq. (A3) gives an equation

$$K_a(\theta)\partial^2_{xx}\theta+\tfrac{1}{2}\Delta K\sin 2\theta(\partial_x\theta)^2 + \frac{\epsilon_a}{8\pi}\left[E_x^2\sin 2\theta-\frac{K_b(\theta)\theta}{K_b(\theta_0)\theta_0}(E'_{0x})^2\sin 2\theta_0\right]\approx 0 \tag{A5}$$

for $\theta=\theta(x,d/2)$ on the interval $0\leqslant x\leqslant\Delta_w$, where $\theta_0=\theta(\Delta_w,d/2)$.

After substituting here E_x from Eq. (31) and multiplying Eq. (A5) by $\partial_x\theta$ this equation can be rewritten as

$$\frac{1}{2}\frac{d}{dx}[K_a(\partial_x\theta)^2]-\frac{\epsilon_a(E'_{0x})^2}{16\pi}\frac{d}{dx}f(\theta)\approx 0 \tag{A6}$$

where

$$f(\theta)\approx\frac{(a-\cos 2\theta_0)^2}{a-\cos 2\theta}+\frac{\sin 2\theta_0\theta^2}{\theta_0}. \tag{A7}$$

We have used $K_b(\theta)/K_b(\theta_0)\approx 1$ for simplicity because this ratio is a slow function of θ and the second term with this ratio in Eq. (A5) is much smaller than the first term in the square brackets for $\theta\ll\theta_0$. Taking into account that for x close to Δ_w x derivatives can be neglected, Eq. (A6) can be integrated and the constant of integration determined, giving

$$\frac{d\theta}{dx}\approx E'_{0x}\left(\frac{\epsilon_a}{8\pi K_a}\right)^{1/2}[f(\theta)-f(\theta_0)]^{1/2}. \tag{A8}$$

[Here $f(\theta)-f(\theta_0)\geqslant 0$ for all θ and θ_0 in the interval $0\leqslant\theta\leqslant\theta_0\leqslant\pi/2$ and $f(\theta)-f(\theta_0)=0$ only if $\theta=\theta_0$.] Substituting dx from this equation into Eq. (A2), one finds that

$$\delta x=\frac{1}{2E'_{0x}}\left(\frac{8\pi K}{\epsilon_a}\right)^{1/2}\int_0^{2\theta_0}dy\left(\frac{1-\delta K\cos y}{f(y/2)-f(\theta_0)}\right)^{1/2} \times\frac{\cos y-\cos 2\theta_0}{a-\cos y}, \tag{A9}$$

where $K=(K_1+K_3)/2$ and $\delta K=(K_3-K_1)/(2K)$. Finally δx and $\mathbf{E}'_0$ can be found self-consistently as was described after Eq. (32). As our calculations show, only three or four iterations are needed to find δx and $\mathbf{E}'_0$ with an error of less than 0.1%.

In this way, however, one has to solve the dynamic equation (4) after each iteration, because θ_0 in Eq. (A9) is unknown from the beginning. To avoid the necessity of solving Eq. (4) repeatedly, we propose another way to calculate θ_0. The main idea is to solve Eq. (22) at $x=\Delta_w$ to estimate θ_0 as the maximum value of $\theta(\Delta_w,z)$ along the z coordinate. In the course of solving Eq. (22), one can take $E_x=E'_{0x}$ and use $E_z(\Delta_w,z)\approx 0$ as was discussed after Eq. (29). To solve Eq. (22), let us divide the gap between substrates at $x=\Delta_w$ into two intervals Δ_1 and Δ_2, where

$$\Delta_1(\Delta_w)+\Delta_2(\Delta_w)=d \quad\text{and}\quad \partial_z\theta=0 \quad\text{at}\quad z=\Delta_1(\Delta_w). \tag{A10}$$

Again, because E'_{0x} is a weak function of z, it is possible and convenient to substitute E'_{0x} by its value $\overline{E'_{0x}}$ averaged over the z coordinate for each interval. After multiplying Eq. (22) by $\partial_z\theta$ and solving the resulting equation using the boundary conditions $\theta(\Delta_w,0)=\theta(\Delta_w,d)=0$ and $\partial_z\theta[\Delta_w,z=\Delta_1(\Delta_w)]=0$ for each interval, one finds the following solutions:

$$\int_0^\theta dw\left[\frac{K_b(w)}{[f_{1,2}(w)-f_{1,2}(\theta_0)]}\right]^{1/2}=\left(\frac{\epsilon_a}{8\pi}\right)^{1/2}\Delta_{1,2}t. \tag{A11}$$

Indices 1 and 2 correspond to a particular interval, t is the normalized z coordinate in each layer: $0\leqslant t\leqslant 1$, where $t=1$ corresponds to the border between the intervals. Functions $f_{1,2}=(e_{1,2})^2\cos 2w$ arise after taking the first integral of the resulting equation, where $e_{1,2}\equiv\overline{E'_{0x1,2}}$ for each interval. Evaluating the two Eqs. (A11) at the point $t=1$ where $\theta=\theta_0$, and summing them, an equation of self-consistency for θ_0

$$\int_0^{\theta_0}dw\left[\frac{K_b(w)}{[f_1(w)-f_1(\theta_0)]}\right]^{1/2}+\int_0^{\theta_0}dw\left[\frac{K_b(w)}{[f_2(w)-f_2(\theta_0)]}\right]^{1/2} =\left(\frac{\epsilon_a}{8\pi}\right)^{1/2}d \tag{A12}$$

is obtained. Equation (A12) is solved with respect to θ_0 after each iteration in the course of finding δx and $\mathbf{E}'_0$ self-consistently.

[1] S. H. Lee, H. Y. Kim, Y. H. Lee, I. C. Park, B. G. Rho, H. G. Galabova, and D. W. Allender, Appl. Phys. Lett. **73**, 470 (1997).
[2] G. Panasyuk and D. W. Allender, J. Appl. Phys. **87**, 649 (2000).
[3] H. Mori, E. C. Garland, Jr., J. Kelly, and P. Bos, Jpn. J. Appl. Phys., Part 1 **38**, 135 (1999).
[4] W. Liu, J. Kelly, and J. Chen, Jpn. J. Appl. Phys., Part 1 **38**, 2779 (1999).
[5] P. G. de Gennes and J. Prost, *The Physics of Liquid Crystals* (Oxford Science, New York, 1993), see Eqs. (3.89) and (5.32).
[6] S. Dickmann, Ph.D. dissertation, University Karlsruhe, Karlsruhe, Germany, 1995.
[7] J. E. Anderson, P. J. Bos, C. Cai, and A. Lien, SID Symp. Dig. **30**, 628 (1999).
[8] W. H. Press, B. P. Flannery, S. A. Teukolsky, and W. T. Vetterling, *Numerical Recipes in C* (Cambridge University Press, Cambridge, England, 1988).

[9] D. Haas, H. Wohler, M. W. Fritsch, and D. A. Mlynski, SID Symp. Dig. **21**, 301 (1990).
[10] H. L. Ong and R. B. Meyer, J. Opt. Soc. Am. A **2**, 198 (1985).
[11] H. L. Ong, J. Appl. Phys. **64**, 614 (1988).
[12] H. L. Ong, J. Appl. Phys. **64**, 4867 (1988).
[13] M. V. Kurik and O. D. Lavrentovich, Sov. Phys. Usp. **31**, 196 (1988).
[14] M. Kleman, *Points, Lines and Walls* (Wiley, New York, 1983).
[15] I. F. Lyuksyutov, Sov. Phys. JETP **48**, 178 (1978).